Available online at www.sciencedirect.com
ScienceDirect
Mathematics and Computers in Simulation ▮ (▮▮▮▮) ▮▮▮–▮▮▮
MATHEMATICS AND COMPUTERS IN SIMULATION
www.elsevier.com/locate/matcom

Original articles

Integrated analysis of the potential, electric field, temperature, pH and tissue damage generated by different electrode arrays in a tumor under electrochemical treatment

Alejandro Soba[a,*], Cecilia Suárez[b], Maraelys Morales González[c], Luis Enrique Bergues Cabrales[d], Ana Elisa Bergues Pupo[e], Juan Bory Reyes[f], José Pablo Martínez Tassé[e]

[a] *CNEA, Argentina*
[b] *Instituto de Física del Plasma, Facultad de Ciencias Exactas y Naturales, Universidad de Buenos Aires - CONICET, Buenos Aires, Argentina*
[c] *Departamento de Farmacia, Facultad de Ciencias Naturales, Universidad de Oriente, Santiago de Cuba, Cuba*
[d] *Dirección de Ciencia e Innovación, Centro Nacional de Electromagnetismo Aplicado (CNEA), Universidad de Oriente, Santiago de Cuba, Cuba*
[e] *Departamento de Física, Facultad de Ciencias Naturales, Universidad de Oriente, Santiago de Cuba, Cuba*
[f] *ESIME-Zacatenco, Instituto Politécnico Nacional, Ciudad de México, DF 07738, Mexico*

Received 15 March 2017; received in revised form 15 September 2017; accepted 16 November 2017
Available online xxxxx

Highlights

- Simulation tool of the partial differential equations of two dimensional models in cancer.
- Calculation and simulations of the potential, electric field intensity, temperature and pH in the tumor.
- Integrated analysis to select adequately an electrode array for tumors.

Abstract

The Electrochemical treatment can be used for local control of solid tumors in both preclinical and clinical studies. In this paper, an integrated analysis of the spatial distributions of the electric potential, electric field, temperature and pH together with the acidic and basic areas are computed, via Finite Element Methods, to improve the geometrical description of electrode arrays for a better electrochemical treatment. These physical quantities are generated by different polarization modes and shapes of electrode arrays. Additionally, the equations over a rectangular two-dimensional domain, which represents the tumor tissue, are solved. The results demonstrate how the electric potential, electric field, temperature and pH distributions depend strongly on the electrode array. Furthermore, significant pH changes and temperature increments are shown after 60 min of treatment. The numerical results agree with the analytical ones reported in the literature. It is concluded that the numerical solution method permits to make an integral analysis, prediction and rapid visualization of the most important electrochemical variables that take place in

* Correspondence to: Comision Nacional de Energia Atomica-CONICET, Av. Gral Paz 1499, Buenos Aires, Argentina.
E-mail address: soba@cnea.gov.ar (A. Soba).

https://doi.org/10.1016/j.matcom.2017.11.006

tumor destruction, thus, providing the possibility of a more effective therapeutic planning before electrochemical treatment is conducted.

Keywords: Electrode arrays; Electric field intensity; pH fronts; Tissue damage

1. Introduction

Electrochemical treatment (EChT) and electrochemotherapy (ECT) are simple, safe, effective, and minimally traumatic for patients with cancer. Furthermore, these treatments induce few side effects in the organism and they can be used when solid tumors cannot be resected after thoracotomy and are not responsive to chemotherapy or radiotherapy, i.e., conventionally inoperable. EChT consists in the application of a low-level direct electric current to the tumor through implanted electrodes [8,26]. ECT, on the other hand, is the electroporation, short electric pulses of high-voltage delivery associated with chemotherapy used to increase drug uptake significantly into the cell by the electro-permeabilization of its membrane [30,47].

These therapies are being intensively studied and applied at present, even at the clinical level. In order to analyze and improve potential EChT applications in clinics, there are necessary deeper studies about basic mechanisms of action as well as the mode of establishing dose–response relationships and confident outcome prediction. In addition, different electrode placements are used and optimal electrode distribution has not been determined yet [41]. In this sense, many authors address their efforts to propose two-dimensional (2D) and three-dimensional (3D) analytical and numerical models in order to improve the geometrical description of electrode arrays [1,3,2,11,37,40,42,41,58].

2D and 3D models have mainly focused on the spatial distributions of the electric potential (Φ), electric field intensity (E) and temperature (T) generated by different electrode arrays [3,30,42,57]. Nevertheless, the adequate selection of an electrode array is based on the analysis of Φ and E [3,42]; T [57]; or Φ, E and T coupled [30]. 2D and 3D models have been indistinctly used in EChT and ECT and their results demonstrate that Φ, E and T spatial distributions depend on tumor characteristics (i.e., size, shape and electrical properties) [25,27,35,51,56] and therapy parameters electrode array geometry (number, shape, location and polarity of electrodes, voltage applied to the electrodes (Vo), number, duration and frequency of pulses) [14,26,29,30,44,56,58]. Tumor electric conductivity increases with the electric field and temperature during EChT/ECT application [13,14,18,30,41,47].

The preclinical and clinical studies demonstrate that Φ, E and T are not only involved in the destruction of solid tumor but also pH change around electrodes. This later has been accepted as the main EChT antitumor mechanism [52]. Electrochemical process [32], protein electro-denaturation fronts [39] and pH fronts [48] during EChT/ECT are reported.

The above-mentioned suggests that the individual analysis of Φ, E and T spatial distributions constitutes a necessary but not sufficient condition for choosing a given electrode array. Both 2D and 3D analytical and numerical models reported in the literature do not deeply discuss how the pH spatial distributions and the changes in time of the acidic and basic areas depend on the electrode array shape.

The aim of this paper is to present a novel and integrated numerical model that describes how Φ, E, T and pH spatial distributions, and acidic and basic areas change with the electrode array geometry during EChT and ECT applications. For this, electrode arrays with circular, elliptic, parabolic and hyperbolic shapes are used, as reported in [42]. Furthermore, Φ and E spatial distributions are compared with those previously reported in [3,42].

2. Model description

2.1. Model assumptions

It is assumed that:

1. 6 electrodes (three positive electrodes-named anodes and three negative electrodes-named cathodes) are placed on electrode array with circular, elliptical, parabolic or hyperbolic shape (Fig. 1).

Please cite this article in press as: A. Soba, et al., Integrated analysis of the potential, electric field, temperature, pH and tissue damage generated by different electrode arrays in a tumor under electrochemical treatment, Mathematics and Computers in Simulation (2017), https://doi.org/10.1016/j.matcom.2017.11.006.

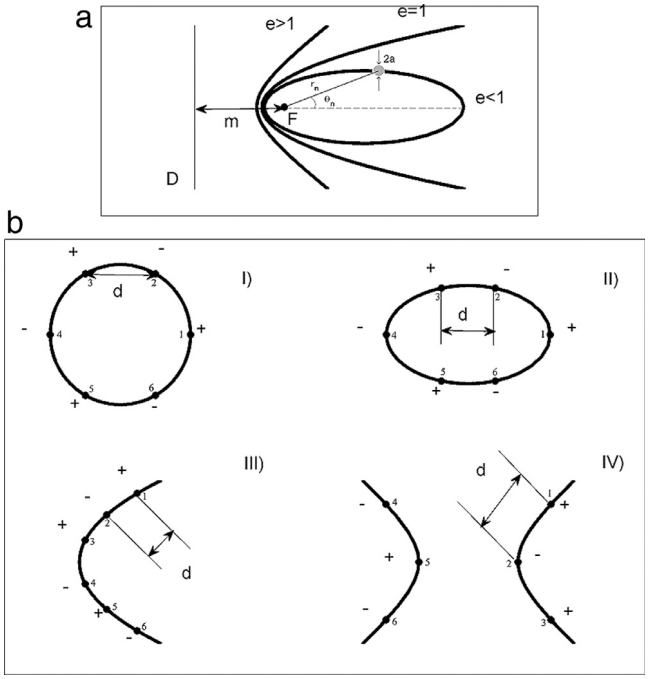

Fig. 1. Electrode configurations. (a) Conic sections: circle ($e = 0$), ellipse ($e < 1$), parabola ($e = 1$) and hyperbola ($e > 1$). (b) Electrode arrays tested in the model. Circle (I), ellipse (II, $e = 0.85$), parabola (III, $e = 1$) and hyperbola (IV, $e = 2$). F, D, a, m, r_n and θ_n are defined in Section 2.4. d the smallest distance between two consecutive electrodes with alternate polarities. Positive and negative electrodes are specified by the + and − signs, respectively.

2. The physical quantity Φ can be considered 2D away from the tips of the electrodes (long, uniform thickness and fully inserted into the superficial tumor). Therefore, it is possible to examine Φ distribution on a plane [3,2,42]. Besides, E spatial distributions in 3D models with needle electrode arrays are similar to the values obtained in 2D [1].
3. A 2D conductive, linear, homogeneous, isotropic medium (tumor) is modeled. This assumption is a simplification commonly accepted in this kind of models, as in other 2D [11,42] and 3D [30] models. The tumor is considered as a single medium by two main reasons: first, the major alterations produced by EChT and ECT occur inside it [25,32,51]. Furthermore, tissue damage occurs mainly around and between electrodes, as in tumors [9,12,40,51] and potato [20,47]. Second, histopathological findings [25] and theoretical simulations [2,26] reveal that the surrounding healthy tissue is minimally affected during and after EChT/ECT. This is not significant for the treatment because E induced in this tissue is low [12,26,42] and the electric current density in healthy tissue is smaller than 10 mA/m^2 [26] due to its high electrical impedance.
4. Tissue relative electrical permittivity and the magnetic induction effect are neglected as non-dominant effects.
5. The anode and cathode are considered H^+ and OH^- sources, respectively.

2.2. Electrode polarization modes

For simulations, three electrode polarization modes are used. Mode 0 consists in two positive upper electrodes (2 and 3), two negative bottom electrodes (5 and 6) and two neutral central electrodes (1 and 4) (see electrode numeration in Fig. 1). Mode 1 is alternated polarization between consecutive electrodes (Fig. 1b). Mode 2 consists in three consecutive electrodes with the same polarity and the other three with the opposite one. For parabolic/hyperbolic arrays, mode 1 alternates polarization between electrodes. On the contrary, mode 2 keeps one polarization in one branch of the parabola/hyperbola, and the opposite in the other branch.

Please cite this article in press as: A. Soba, et al., Integrated analysis of the potential, electric field, temperature, pH and tissue damage generated by different electrode arrays in a tumor under electrochemical treatment, Mathematics and Computers in Simulation (2017), https://doi.org/10.1016/j.matcom.2017.11.006.

2.3. Electric potential, electric field, temperature and pH spatial distributions

Mode 1 is used for simulations of Φ (in V), E (in V/cm), T (in °C) and pH spatial distributions generated by these four electrode array shapes for 1 h of treatment. The equations to calculate Φ (solution of Poisson nonlinear equation for the entire region outside the electrodes), Eq. (1); E (gradient of scalar electric potential), Eq. (2); T (stationary bioheat equation), Eq. (3) and pH (diffusion equation, see Eq. (4)) are given by

$$\nabla \bullet (\sigma(E, T)\nabla \Phi) = 0 \tag{1}$$

$$\vec{E} = -\nabla \Phi \tag{2}$$

$$\nabla \bullet (k\nabla T) - w_b c_b \rho_b (T - T_a) + q''' + \sigma(E, T)|\nabla \Phi|^2 = 0 \tag{3}$$

$$\nabla \bullet (D_i \nabla C_i) = \frac{\partial C_i}{\partial t} \tag{4}$$

with

$$\sigma(E, T) = \sigma_0 [1 + \sigma_E(E) + \sigma_T(T)] \tag{5}$$

$$\sigma_E(E) = \begin{cases} 3.5 & E > E_{irrev} \\ 1.0 + 2.5\dfrac{E - E_{rev}}{E_{irrev} - E_{rev}} & E_{irrev} \geq E \geq E_{rev} \\ 1.0 & E_{rev} > E \end{cases} \tag{6}$$

and

$$\sigma_T(T) = a_T [T - T_a] \tag{7}$$

where $\sigma(E, T)$ is the mean electric conductivity of the tumor during EChT/ECT [18] whereas σ_0 is its mean basal electrical conductivity. $\sigma_E(E)$ and $\sigma_T(T)$ are the average electrical conductivities due to E and T induced in this tissue by EChT/ECT, respectively [47]. E_{rev} (230 V/cm) is the reversible electric field intensity. E_{irrev} (350 V/cm) is the irreversible electric field intensity [10]. a_{T} (0.032 °C^{-1}) is a temperature coefficient that depends on the thermal characteristics of the material (a generic biological tissue in this case) [18]. T_a is the arterial temperature (37 °C). k (0.564 W m^{-1} K^{-1}), c_b (3840 J kg^{-1} K^{-1}), ρ_b (1039 kg m^{-3}), w_b (0.00715 s^{-1}) and q''' (10.437 W m^{-3}) represent the tissue thermal conductivity, specific heat capacity, mass density of the blood, blood perfusion rate and the metabolic heat generation rate (all living tissue generates heat by the inner metabolic activity of the cells that constitutes the tissue), respectively [18]. D_i means the diffusion coefficient of the species i (H^+ and OH^-) whereas C_i is the concentration of these species. t denotes the time. These two ionic species are selected because during electric stimulation, the electrons react with water molecules at the cathodic side to produce hydroxyl ions, while at the anodic side, protons are formed. Thus, gradients of H^+ and OH^- ions across the tissue are formed between the anodic and cathodic interface.

For the simulations, the potential applied to the electrodes (Vo) is 12 V (+6 V to anodes and −6 V to cathodes) [27]. Vo is applied during 1 h. The distance d between adjacent electrodes is 0.5 cm, as in preclinical studies [18,44] in order to compare our results with those reported in [42]. $\sigma_0 = 0.4$ S/m [36], and $C^0_{H^+} = 1 \times 10^{-7}$ mol/dm^3, $C^0_{OH^-} = 1 \times 10^{-7}$ mol/dm^3, $D_{H^+} = 6.25 \times 10^{-5}$ cm/s and $D_{OH^-} = 3.52 \times 10^{-5}$ cm/s [49] are used. Superscript 0 indicates initial concentration of specie i. All electrical conductivities are given in S/m.

The Pennes bioheat equation is the most accepted to calculate heat transfer in tissues [30]. Despite, Eq. (3) is used because Vo is direct and temperature transitory variations that appear during the first moments of therapy application are neglected in regard to the thermal effects induced in the tumor by Vo application. Moreover, variations of T exhibit mainly due to the non-linearity and introduced in $\sigma(E, T)$ coefficients, as reported by Lacković et al. [30]. When time elapses, $\sigma(E, T)$ coefficients change by the tumor electrical property modifications because E and T are modified due to Vo application [18,47].

Eq. (4) considers hydrogen ions (H^+) involve in the acidic pH and in water electrolysis ($2H_2O \leftrightarrow O_2 + 4H^+ + 4e^-$) around the anode. Besides, this equation takes into account hydroxide ions (OH^-) involve in the alkaline pH and in water electrolysis ($2H_2O + 2e^- \leftrightarrow H_2 + 2OH^-$) around cathode, during EChT [32,36]. The acidic pH and basic pH are explained by the formations of hydrochloric acid ($H^+ + Cl^- \rightarrow HCl$) and sodium hydroxide

Please cite this article in press as: A. Soba, et al., Integrated analysis of the potential, electric field, temperature, pH and tissue damage generated by different electrode arrays in a tumor under electrochemical treatment, Mathematics and Computers in Simulation (2017), https://doi.org/10.1016/j.matcom.2017.11.006.

($N_a^+ + OH^- \rightarrow N_aOH$), respectively. Sodium and chlorine ions are formed from the decomposition of sodium chloride ($N_aCl \rightarrow N_a^+ + Cl^-$) [32]. Mobilities and concentrations of H^+ and OH^- species modify their diffusion coefficients.

For each electrode array shape in mode 1 and for 1 h of EChT/ECT, pH spatial distributions around anodes and cathodes are shown separately to examine how pH distributes around positive electrodes or negative electrodes. Additionally, an average pH in each point (x, y) generated by all electrodes, for each electrode array shape, is given to know how each tumor area is affected or not under EChT action. The tumor area is affected if $0 \leq$ average pH ≤ 6 or $7 \leq$ average pH ≤ 14. Conversely, the tumor area is not affected if $6 <$ average pH < 7.

2.4. Finite element methods

Finite Element Methods (FEM) are used to obtain the numerical solution of Eqs. (1)–(4) on a 2D rectangular domain $10d \times 5d/10d \times 5d$ (where d is the electrode distance). The size of this rectangular domain is 5×2.5 cm and guarantees that tumor boundary (Σ) is far enough and does not disturb the solution of the problem. In this study, the treated area (tumor tissue plus margin security area) is defined by the area covered by threshold E, pH or T values. With the electrode configurations that are used here, tumor size is in the order of the square centimeter, a very realistic tumor size [25]. This rectangular domain size is sufficient to know 2D spatial distributions of Φ, E, T and pH around and between electrodes, as well as in zones away from them. It should be noted that all electrode arrays are inserted inside this 2D rectangular domain. The mesh of 60 000 nodes is uniform with a mean size of element $d/10$ (0.05 cm). The electrodes are considered as points because their diameters are lower than a node of the mesh and this FEM code does not take into account the electrode radius.

The weak formulation is more general and allows an optimal treatment of the boundary conditions involving derivatives. This numerical code is based on this formulation and allows treating Dirichlet conditions or other natural ones easily. The Galerkin formulation is built on this weak formulation and an adequate mesh. Furthermore, this weak formulation is applied to Eqs. (1), (3) and (4) to calculate Φ, T and C_i, respectively. This is important to simultaneously know how these three quantities and E are affected for each electrode array shape. This allows an adequate selection of electrode array shape. A set of standard discrete equations of the forms $K(\phi^{i-1})\phi^i = f(\phi^{i-1})$ (for Φ and T) and $K\phi^{n+1} = M\dot{\phi}$ (for C_i) results from this weak formulation. Eqs. (1) and (3) are coupled by the Joule heating term (or heating power per unit volume, represented by $\sigma(E, T)|\nabla\Phi|^2$) that appears in Eq. (3) [13,30]. Together with appropriate boundary and initial conditions, Eqs. (1) and (3) represent a complete formulation of the problem in the form of two coupled partial differential equations. These equations are simultaneously solved by the Picard iterative method [43,54]. Stable solutions for T and E are reached for seven iterations. When $\sigma(E, T)$ increases with T (see Eqs. (5) and (7)), as in other works [30,36], additional coupling between Eqs. (1) and (3) exists (see Eqs. (5)–(7)). Eq. (4) is solved by the Crank–Nicolson iterative method [16], reaching its stable solution for seven iterations.

Eqs. (1)–(4) are coupled because Vo appears at their prescribed electrode boundaries. Eqs. (1) and (2) are solved for prescribed voltage boundary conditions on the electrodes and insulating boundary conditions on the outer edges of the domain. Eq. (3) is solved under boundary conditions of null flux and parameters reported in previous studies [18,53]. On the other hand, Eq. (4) is solved under boundary conditions of null flux together with the parameters mentioned above [49]. Acidic and basic pH values are calculated in each finite element on the basis of concentrations H^+ ($-\log_{10}$ [H^+]) and OH^-($-\log_{10}$ [OH^-]), respectively.

Pupo et al. [42] use the unifying principle for conic sections to calculate the leading-order potential ($\Phi^0(z)$) and the leading-electric field intensity ($E^0(z)$) in an equidistant distribution of electrodes over a conic curve, given by

$$\Phi^0(z) = \sum_{n=1}^{N} C_n \ln\left(\frac{a}{z - z_n}\right), \tag{8}$$

$$E^0(z) = \sum_{n=1}^{N} C_n \left(\frac{a}{z - z_n}\right), \tag{9}$$

with

$$z_n = r_n e^{i\varphi_n} \tag{10}$$

$$r_n = \frac{me}{1 \pm e\cos\theta_n}, \tag{11}$$

Please cite this article in press as: A. Soba, et al., Integrated analysis of the potential, electric field, temperature, pH and tissue damage generated by different electrode arrays in a tumor under electrochemical treatment, Mathematics and Computers in Simulation (2017), https://doi.org/10.1016/j.matcom.2017.11.006.

where N represents the total number of electrodes placed on the array and z is the position of the point where the calculations are made. a is the electrode radius. z_n is the position of the nth electrode of the array. m is the distance between the focus (F) and the directrix line (D), as shown in Fig. 1a. The straight line passing through F and perpendicular to D is assumed to be the prime direction, from which the angles are measured. r_n and θ_n are the polar coordinates of the nth electrode (with the origin on the point F). The parameter e is the conic eccentricity that distinguishes the type of conic section: $e = 0$ (the locus is a circle), $e < 1$ (the locus is an ellipse), $e = 1$ (the locus is a parabola) and $e > 1$ (the locus is a hyperbola) [42].

In Eqs. (8) and (9), C_n are constants to be determined from the boundary conditions, which may be determined by solving non-homogeneous system of linear equations (see details in Aguilera et al. [3] and Pupo et al. [42]). Consequently, C_n depends on potential on the jth electrode ($j = 1, \ldots, N$). Besides, in Eq. (8), a constant term is added if the number of electrodes is odd to satisfy conservation of the current [11]. r_n can easily be shown to have a general expression in polar coordinates similar in the three curves if the origin of coordinates is located in the conic focus. It should be remarked that in the case of a hyperbola this equation represents only one of its branches (the one whose focus is at the origin), rather than the entire curve. The plus sign corresponds to the left branch of the hyperbola [42].

Aguilera et al. [3] proposed a complex variable ($z = x + iy$) and demonstrate that the total electric potential can be written as a sum of multi-poles of all electrodes. The higher terms in multipole series can be neglected as the distance between electrodes is larger than the electrode radius. So, $\Phi^0(z)$ and $E^0(z)$ can be used. These authors also showed that the multipole series for the electric potential and the electric field agree well.

To test the validity of this numerical code, Φ and E spatial distributions are compared with $\Phi^0(z)$ and $E^0(z)$ reported by Pupo et al. [42] (for four electrode array shapes and mode 1). Besides, Φ and E are compared with $\Phi^0(z)$ and $E^0(z)$ reported by Aguilera et al. [3]. This comparison is made for the electrode arrays with circular ($e = 0$) and elliptical ($e = 0.85$) shapes, and mode 0, and along three different paths: (1) through electrodes 6 and 2; (2) through electrodes 4 and 1; and (3) through electrodes 3 and 2 (Fig. 1). For $\Phi^0(z)$ and $E^0(z)$ simulations, $a = 0.215$ mm is considered [3].

2.5. Relative acidic and basic areas

The relative acidic area around anode (ratio of the tumor area with pH ≤ 6 relative to the total tumor area, A_{acidic}) and the relative basic area around cathode (proportion of the tumor area with pH ≥ 8 relative to the total tumor area, A_{basic}) are computed for estimating the tumor necrosis area induced by anodes and cathodes. A_{acidic} vs. t ($A_{\text{acidic-t}}$) and A_{basic} vs. t ($A_{\text{basic-t}}$), during 1 h of EChT/ECT, are also shown to determine how the tumor necrosis area changes over time during therapy.

2.6. Other simulations for the four electrode arrays in modes 1 and 2

The maximum T ($T_{\max}$) versus Vo and maximum E ($E_{\max}$) versus Vo generated by different electrode array modes are studied. Electrode array modes are circular mode 1 (A1), circular mode 2 (A2), elliptic mode 1 (A3), elliptic mode 2 (A4), parabolic mode 1 (A5), parabolic mode 2 (A6), hyperbolic mode 1 (A7) and hyperbolic mode 2 (A8) arrays. These modes are compared by means of $T_{\max}$ versus Vo, $E_{\max}$ versus Vo, $A_{\text{acidic-t}}$ and $A_{\text{basic-t}}$. These simulations and comparisons are made for 1 h of EChT/ECT and varying Vo in the experimental range (2 to 12 V) [27,56].

2.7. Comparison criteria

The maximum difference ($D_{\max}$) and the Root Means Square Error (RMSE) are used for the comparison, given by

$$D_{\max} = \max |F_i - G_i| \tag{12}$$

$$\text{RMSE} = \sqrt{\sum_{i=1}^{M} \frac{(F_i - G_i)^2}{M}}. \tag{13}$$

M (number of points), G_i and F_i depend on the comparison performed. When the results of the FEM code are compared with those reported by Pupo et al. [42], $M = 33\,000$ points inside each electrode array and G_i and F_i are

Please cite this article in press as: A. Soba, et al., Integrated analysis of the potential, electric field, temperature, pH and tissue damage generated by different electrode arrays in a tumor under electrochemical treatment, Mathematics and Computers in Simulation (2017), https://doi.org/10.1016/j.matcom.2017.11.006.

the ith calculated values of Φ/E and $\Phi^0(z)/E^0(z)$, respectively. For the case that the data obtained with the FEM code and those reported by Aguilera et al. [3] are computed, $M = 100$ and G_i and F_i are the ith calculated values of Φ/E and $\Phi^0(z)/E^0(z)$ along each path, respectively. When T_{max} vs. Vo plot generated by the four electrode array shapes for modes 1 and 2 are compared among themselves, $M = 6$, G_i are the i-th calculated values of T_{max} for an electrode array and mode given, whereas F_i are those for another electrode array shape and mode specified. This same analysis is also made for E_{max} vs. Vo, $A_{acidic\text{-}t}$ or $A_{basic\text{-}t}$ plot generated by these four electrode arrays and two modes. In these three cases, G_i and F_i have the same interpretation but for E_{max}, A_{acidic} or A_{basic}.

Expressions to calculate the values of Φ, E, $\Phi^0(z)$, $E^0(z)$, T, C_i, pH, A_{acidic}, $A_{acidic\text{-}t}$, A_{basic}, $A_{basic\text{-}t}$, D_{max} and RMSE, and the Picard and Crank–Nicolson iterative methods are implemented by an own code written in Fortran 90/95 language (Fortran 90/95 Programming Manual, Tanja van Mourik, 2005) and executed on a I7-class computer with 8 threads and 8 Gb of Ram memory. Each calculation takes five to ten minutes. For the calculations, millimeter, centimeter and decimeter unities are converted in meter. Moreover, the matrix of Φ, E, T and pH for each electrode array are processed in a 256-core processor HPC with 256 GB RAM, to show their spatial distributions. The figures are shown in GNU Octave 4.0 (free software, License 2015-05-29). As part of the GNU Project, GNU Octave is free software under the terms of the GNU General Public License. The website is http://gnu.org/software/octave. Free Software Foundation funds the GNU Project. Developer(s): John W. Eaton and many collaborators. This machine is acquired by the Flemish Development Cooperation through VLIR-UOS (Flemish Interuniversity Council-University Cooperation for Development of Belgium) in the context of the Institutional University Cooperation programme with Oriente University, Santiago de Cuba, Cuba.

3. Results

Figs. 2–5 show Φ (Figs. 2a–5a), E (Figs. 2b–5b), T (Figs. 2c–5c), basic pH around cathodes (Figs. 2d–5d), acidic pH around anodes (Figs. 2e–5e) and average pH (Figs. 2f–5f) spatial distributions generated by circular, elliptical ($e = 0.85$), parabolic and hyperbolic electrodes arrays, respectively. All these distributions are highly non-homogeneous in the tumor and deeply depend on electrode configuration. These figures evidence that higher modular values for Φ, E ($45 \leq E \leq 50$ V/cm) and T ($7 \leq T \leq 52$ °C) are observed at and around the electrodes and these decrease among electrodes. pH reaches its smallest and greatest values at and around anode (pH ≤ 3) and cathode (pH ≥ 12), respectively. Interestingly, for all electrode arrays, A_{acidic} (pH ≤ 6) and A_{basic} (pH ≥ 8) extend through the tumor area, being more noticeable for A_{acidic}. For the tumor regions away from the electrodes (toward to Σ), Φ and E tend to zero, T decreases up to its physiological value (approximately 37 °C), and pH values tend to neutrality (nearly 7).

Φ and E spatial distributions obtained with the use of FEM code agree with those reported by Aguilera et al. [3], Pupo et al. [42], for all $0 \leq e \leq 2$ and spatial position along paths tested. Fig. 6 shows this good agreement for $e = 0.85$ and three different paths. For the comparison of Φ and $\Phi^0(z)$, $D_{max} = 0.0751$ V and RMSE $= 0.0513$ V (paths through electrodes 6 and 2, Fig. 6a); $D_{max} = 0.0920$ V and RMSE $= 0.0096$ V (paths through electrodes 4 and 1, Fig. 6c); and $D_{max} = 0.0004$ V and RMSE $= 0.0003$ V (paths through electrodes 3 and 2, Fig. 6e). For the comparison of E and $E^0(z)$, $D_{max} = 0.0060$ V/cm and RMSE $= 0.0049$ V/cm ((paths through electrodes 6 and 2, Fig. 6b); $D_{max} = 0.0005$ V/cm and RMSE $= 0.0003$ V/cm (paths through electrodes 4 and 1, Fig. 6d); and $D_{max} = 0.0002$ V/cm and RMSE $= 0.0001$ V/cm (paths through electrodes 3 and 2, Fig. 6f). All these comparisons reveal small values of D_{max} and RMSE. In addition, it can be verified that small values of D_{max} and RMSE are obtained for any paths between two electrodes when $e = 0.85$ and electrode arrays with $0 \leq e \leq 0.99$ (results not shown).

For four electrode arrays and modes 1 and 2, T_{max} and E_{max} values around electrodes non-linearly and linearly increase as Vo increases, respectively (results not shown). Below 4 V, these four electrode arrays generate the same T_{max} values. For $Vo \geq 6$ V, elliptical mode 2 and parabolic mode 1 arrays induce the lowest T_{max} values while the circular mode 1 and the hyperbolic mode 2 arrays induce the highest ones. The elliptical array produces the smallest E_{max} values for all Vo values, and parabolic and hyperbolic arrays mode 2 generate the highest ones. It can be seen in Tables 1 and 2 that T_{max}, E_{max}, A_{acidic} and A_{basic} depend on Vo, electrode array shape and polarization mode for 12 V and 1 h of EChT/ECT. Table 2 shows that parabolic mode 2 and circular mode 2 electrode arrays induce the highest and lowest relative areas, respectively.

$A_{acidic\text{-}t}$ (Fig. 7a) and $A_{basic\text{-}t}$ (Fig. 7b) increase with the time (during 1 h of treatment), for all electrode arrays and modes 1 and 2, being more noticeable for A_{acidic} obtained with parabolic and hyperbolic arrays in both modes 1 and 2. Circular and elliptical arrays for mode 2 induced the lowest values of A_{acidic} and A_{basic}. These results confirm that

Please cite this article in press as: A. Soba, et al., Integrated analysis of the potential, electric field, temperature, pH and tissue damage generated by different electrode arrays in a tumor under electrochemical treatment, Mathematics and Computers in Simulation (2017), https://doi.org/10.1016/j.matcom.2017.11.006.

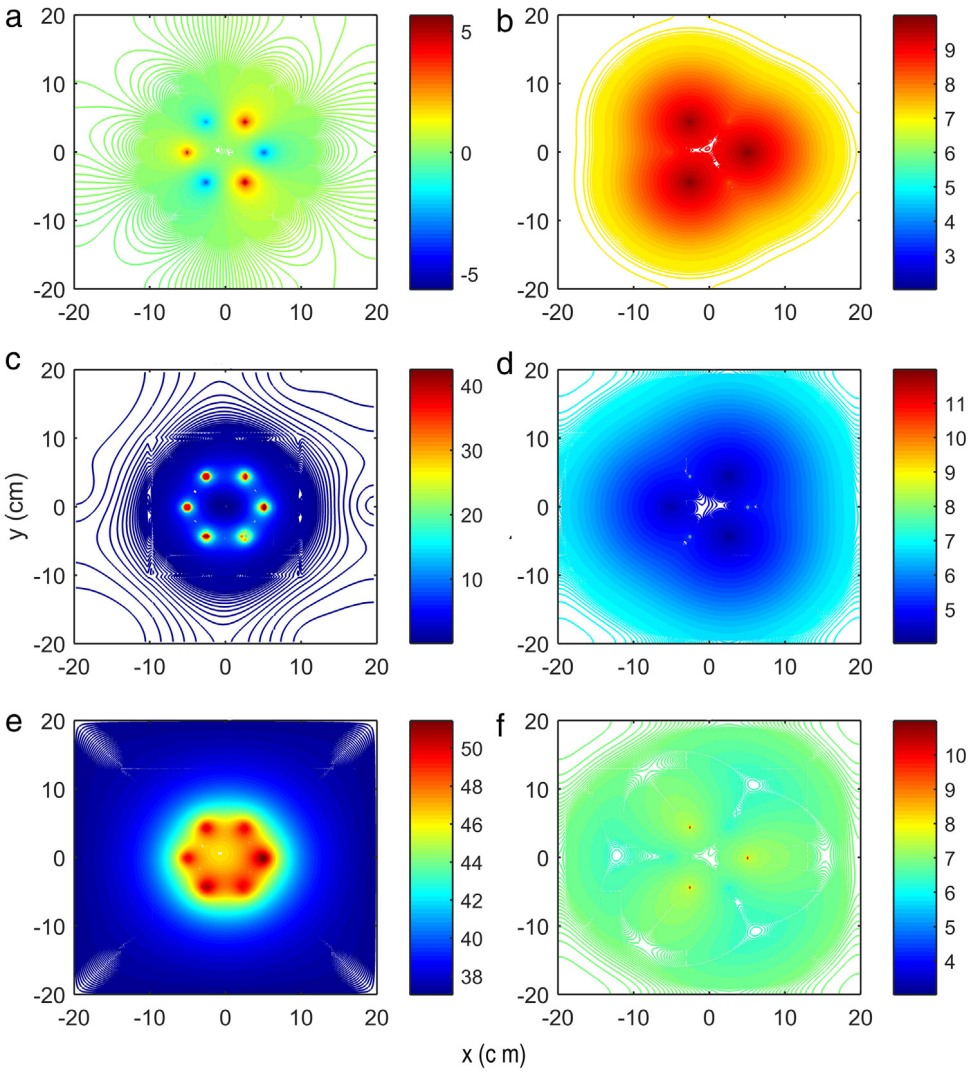

Fig. 2. Spatial distributions of (a) electric potential; (b) electric field intensity; (c) temperature; (d) basic pH around cathodes; (e) acidic pH around anodes and (f) average pH generated by 12 V during 1 h of EChT (ECT) for a circular array of six electrodes in the mode 1.

$A_{\text{acidic-t}}$ proved to be wider than $A_{\text{basic-t}}$ and agree with those shown in Figs. 2d–5d. Furthermore, Fig. 7 reveals that $A_{\text{acidic-t}}$ turns out to be faster than $A_{\text{basic-t}}$. The comparison of these four electrode arrays for modes 1 and 2 shows small values of $D_{\max}$ and RMSE. Although the results are not shown, A_{acidic}, A_{basic}, $A_{\text{acidic-t}}$ and $A_{\text{basic-t}}$ increase non-linearly as Vo increases.

4. Discussion

The main merit of this study is the development of an integrated analysis of the coupling of Vo with Φ; E; T; mobility and concentration of H^+ and OH^- ions; pH; $\sigma(E, T)$; A_{acidic}; A_{basic}; $A_{\text{acidic-t}}$ and $A_{\text{basic-t}}$ parameters; and their effects on cellular death, unprecedented in the literature. From experimental point of view, this integrated analysis requires an excessive handling of animals, expensive resources and a considerable amount of time. The results of this paper are valid for a single stimulus of EChT/ECT, four shapes of electrode arrays (circular, elliptical, parabolic and hyperbolic) and three electrode polarization modes. These agree with those reported in [3,42] and COMSOL-Multiphysics. In addition, these theoretical results confirm that 2D spatial distributions of Φ, E, T and pH depend on electrode array shape, as verified theoretically [42,41] and experimentally in potato [20,47] and tumors [12,40].

Please cite this article in press as: A. Soba, et al., Integrated analysis of the potential, electric field, temperature, pH and tissue damage generated by different electrode arrays in a tumor under electrochemical treatment, Mathematics and Computers in Simulation (2017), https://doi.org/10.1016/j.matcom.2017.11.006.

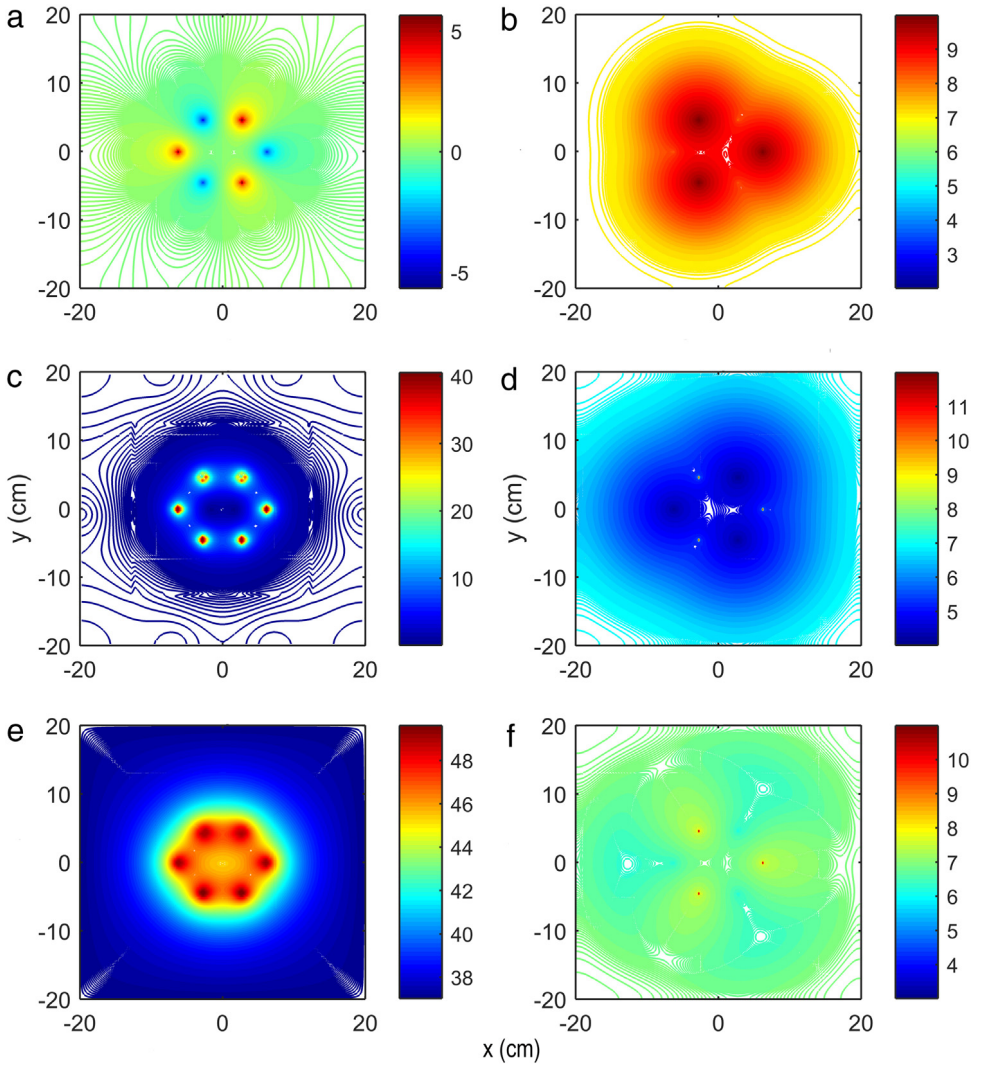

Fig. 3. Spatial distributions of (a) electric potential; (b) electric field intensity; (c) temperature; (d) basic pH around cathodes; (e) acidic pH around anodes and (f) average pH generated by 12 V during 1 h of EChT (ECT) for an elliptical array of six electrodes in the mode 1.

Despite the vast difference of Φ, E, T and pH spatial distributions generated by these electrode array shapes, their respective A_{acidic} and A_{basic} are nearly the same, suggesting that they can be interchangeably used in EChT and ECT in modes 1 and 2. In contrast, electrode arrays with circular and elliptical shapes and electrode hyperbolic array [42] have been suggested to treat cancer. Nevertheless, we should be very careful with these statements because A_{acidic} and A_{basic} are not reported after EChT treatment. A further study is required to describe $A_{\text{acidic-t}}$ and $A_{\text{basic-t}}$ during and after exposure time of EChT. Significant destruction of potato [20] and tumor [8,9,12,25,40,44,52,51,56] is observed after EChT application. Additionally, this potato destruction is also observed when ECT is conducted [40,47].

Acidic pH around anode, basic pH around cathode and unaffected tumor areas away from the electrodes agree with the experimental results [32,51]. It has been experimentally demonstrated that tumor areas that have not been affected by EChT/ECT cause the tumor to re-grow. These areas can be avoided by the use of multiple needle electrodes, as reported in [1,26,29]. Besides, the fact that Φ and E values tend to zero, and T and pH reach their physiological values for regions near Σ explains the minimal adverse effects observed in the surrounding healthy tissue [25,56]. This fact justifies, in part, why a single medium is used, in addition to arguments given in the assumption 3.

Please cite this article in press as: A. Soba, et al., Integrated analysis of the potential, electric field, temperature, pH and tissue damage generated by different electrode arrays in a tumor under electrochemical treatment, Mathematics and Computers in Simulation (2017), https://doi.org/10.1016/j.matcom.2017.11.006.

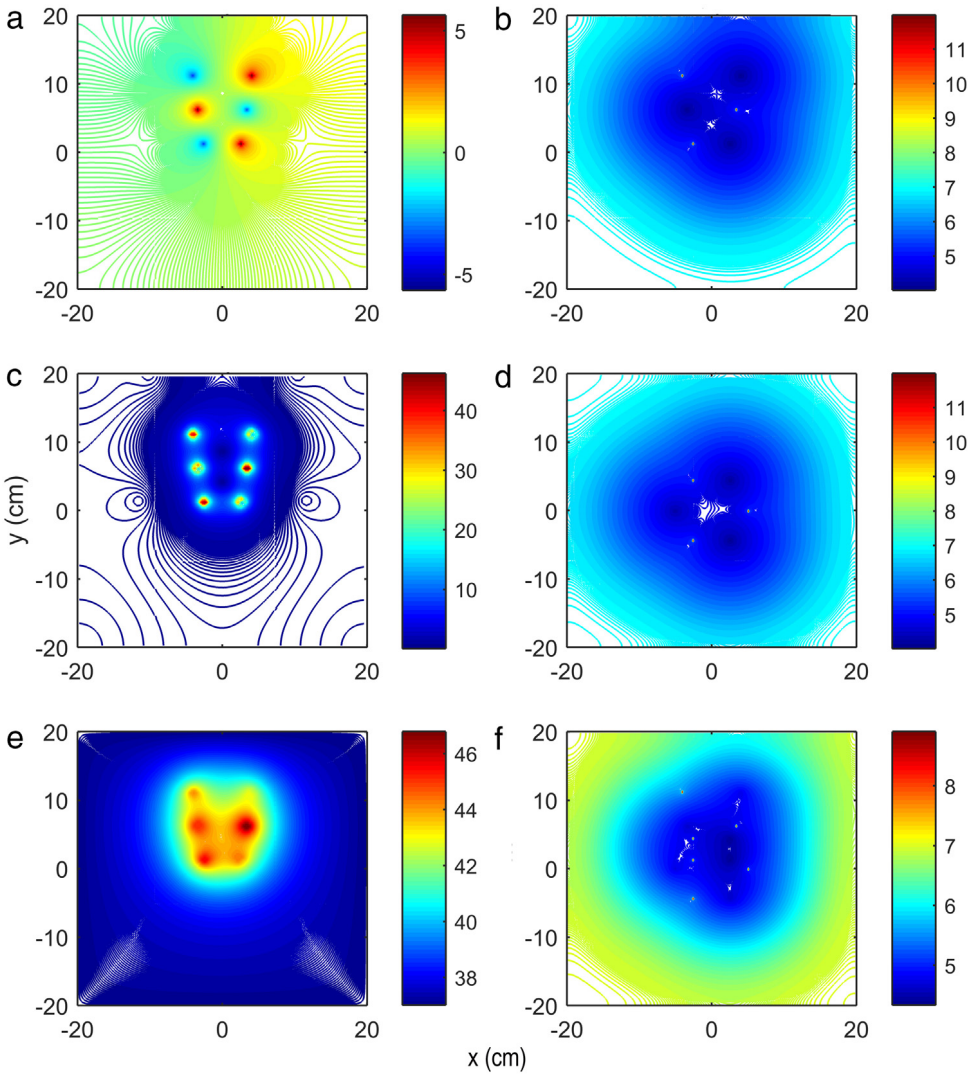

Fig. 4. Spatial distributions of (a) electric potential; (b) electric field intensity; (c) temperature; (d) basic pH around cathodes; (e) acidic pH around anodes and (f) average pH generated by 12 V during 1 h of EChT (ECT) for a parabolic array of six electrodes in the mode 1.

As a result of Vo application, mobility and concentration of H^+ and OH^- ions may be due to water electrolytic decomposition around electrodes [21,28,32] and/or water self-dissociation from dissociation–association processes ($2H_2O \rightarrow H_3O^+ + OH^-$), where H_3O^+ is the hydronium ion [4–7,46]. The formation of H_3O^+ and OH^- ions has been suggested when EChT is applied [21]. Disruption of the water structures between and within cells by necrosis due to EChT/ECT action may be involved in these results, in agreement with Davidson et al. [15]. This fact is in correspondence with the inflammation and edema observed during EChT application and the first days post-treatment [8,9,25].

The induction of H_3O^+/H^+ ions and the hydrochloric acid around anodes may explain A_{acidic}. However, the formation the OH^- ions and sodium hydroxide around cathodes justify why A_{basic}, in agreement with [32,42,48,50]. A_{acidic} and A_{basic} may be influenced by the flux of interstitial water from anode to cathode and other charged ionic species involved in the complex electrochemical processes induced in the tumor. This flux may cause dehydration at the anode and hydration at the cathode, as reported in [12,32].

Electrode polarization may influence over A_{acidic} and A_{basic} by the change in the concentration of the electroactive species at surface electrode, over-potential (by transfer and slowness of the charge transfer process through electrode

Please cite this article in press as: A. Soba, et al., Integrated analysis of the potential, electric field, temperature, pH and tissue damage generated by different electrode arrays in a tumor under electrochemical treatment, Mathematics and Computers in Simulation (2017), https://doi.org/10.1016/j.matcom.2017.11.006.

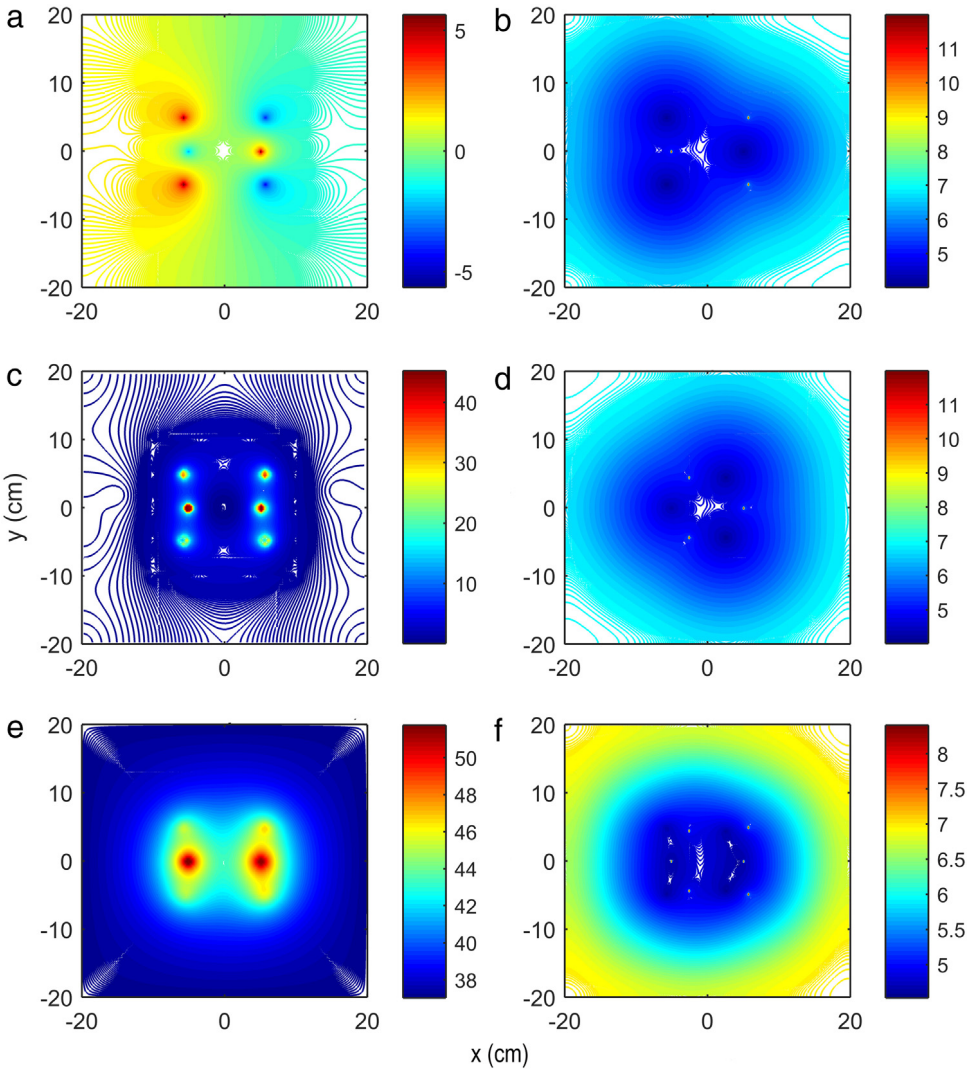

Fig. 5. Spatial distributions of (a) electric potential; (b) electric field intensity; (c) temperature; (d) basic pH around cathodes, (e) acidic pH around anodes and (f) average pH generated by 12 V during 1 h of EChT (ECT) for a hyperbolic array of six electrodes in the mode 1.

interface), reaction over-potential (by the existence of different chemical reactions that happen in the tumor), oxide metal and organic substance layers absorbed over the electrodes [24,28]. These results may be argued because the increase of the concentration of the substance that oxidize in the anodic surface make that the electrode potential of the anode increases and the decrease of the concentration of the substance that reduces at the cathodic surface make the electrode potential of the cathode decreases. In addition, protons under influence of the electric field and the concentration difference should move from anode to cathode.

Stilinger [46] report a significant declination of OH^- (hydrated OH^- ($OH^-(H_2O)_n$)) and an increase of H^+ (hydrated H^+ ($H^+(H_2O)_n$)) when these two types of ions act anomalously under a perturbation (i.e., E, T and pH induced by Vo application), probably by association–dissociation processes in water. Besides, it well known that the size, concentration and mobility of H_3O^+/H^+ ions are smaller, higher and faster than those of OH^- ions, respectively [50], explaining why A_{acidic} is higher than A_{basic} and $A_{\text{acidic-t}}$ is faster than $A_{\text{basic-t}}$. These two results confirm the inverse ratio between concentrations of H^+ and OH^- ions ($[H^+][OH^-] = K_w = 10^{-14}$) and agree with those reported by Olaiz et al. [37]. The fact that the acidic area prevails may impact in antitumor effect during and

Please cite this article in press as: A. Soba, et al., Integrated analysis of the potential, electric field, temperature, pH and tissue damage generated by different electrode arrays in a tumor under electrochemical treatment, Mathematics and Computers in Simulation (2017), https://doi.org/10.1016/j.matcom.2017.11.006.

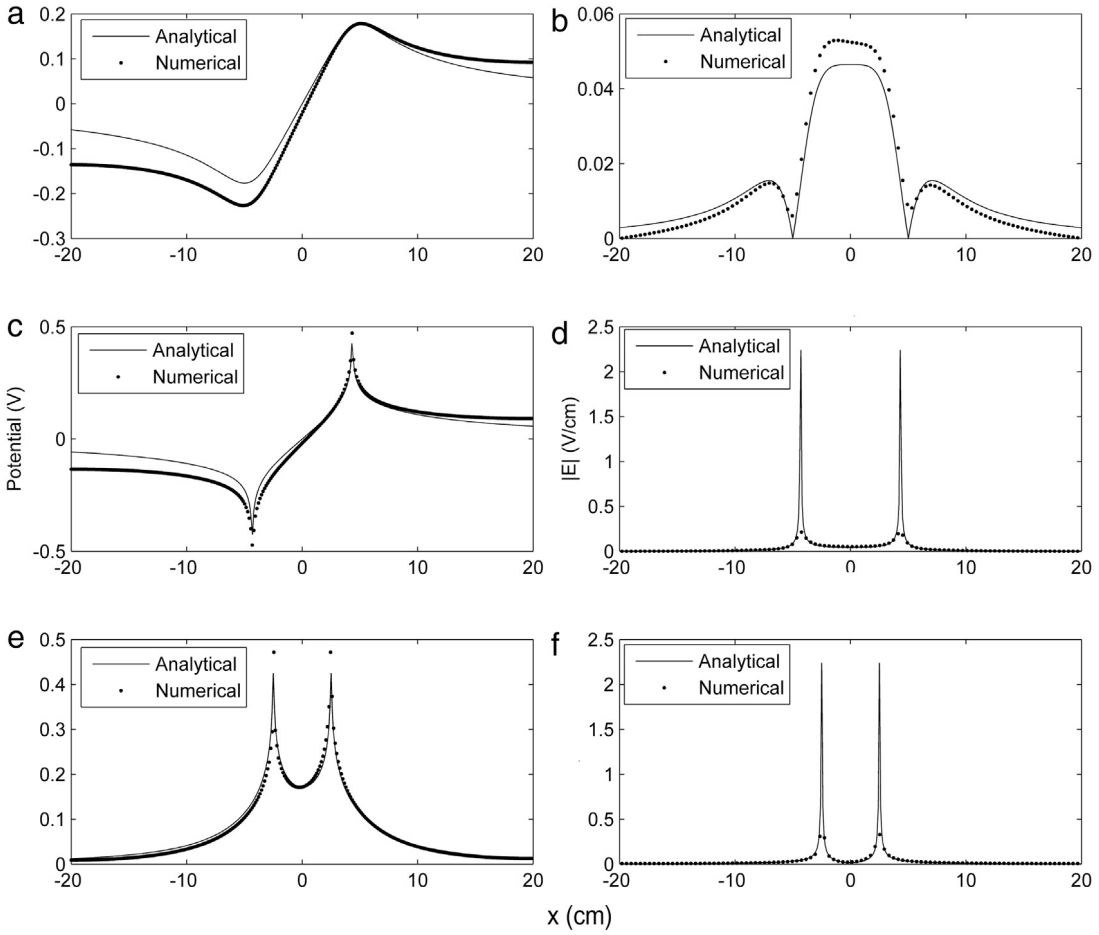

Fig. 6. Solutions obtained with this numerical code (dotted lines) and those reported by Aguilera et al. [3] (solid lines) generated by an electrode elliptical array ($e = 0.85$) in mode 0, for the electric potential (V, left) and electric field intensity (V/mm, right), as function of spatial position along three different paths: (a–b) through electrodes 6 and 2; (c–d) through electrodes 4 and 1 and (e–f) through electrodes 3 and 2. Electrode numeration is shown in Fig. 1. Voltage applied to the electrodes is 12 V for 1 h of treatment. The results of Aguilera et al. [3] contain 401 points and those obtained with this numerical code contain 301 points for Φ and $\Phi^0(z)$ (Fig. 6a,c,e), and 100 points for E and $E^0(z)$ (Fig. 6b,d,f).

after EChT application [52] and in both inflammatory and immune responses [23,31], thus corroborating that a correct manipulation of the tumor pH may have important therapeutic implications, as McCarty and Whitaker [34] reported.

Induction of Φ, E, T and pH in the tumor first produce microscopic damages (at cellular, molecular and electronic levels) that are subsequently observed at macroscopic level (A_{cidic} and A_{basic}). Besides, increase of $A_{\text{acidic-t}}$ and $A_{\text{basic-t}}$ generated by all electrode arrays agree with the increased space-time necrosis area reported in tumors after EChT treatment [8,9,25,52,51] and in potato during EChT [20] and ECT [47], suggesting the validity of these theoretical results.

The temperature T induced in the tumor is due to Joule effect [30,47]. This Joule heating explains the skin erythema in patients [25]. This erythema differs completely from the burn produced by radiotherapy and/or hyperthermia [30]. However, Cury et al. [12] conclude that EChT antitumor effect is by electrochemical processes and not by temperature. Artemov et al. [4–6] suggest that concentrations of H_3O^+ and OH^- do not depend on T. On the other hand, pH decreases and the constant equilibrium for water solution (K_w) increases non linearly when T increases. As a result, the dimensionless activity of the species H_3O^+, OH^- and H_2O depends non-linearly on T [7].

Non-linear rise of $T_{\max}$, linear increase of $E_{\max}$ as well as non-linear space-time enlargement of A_{acidic} and A_{basic} as Vo increases may be connected with non-linear increase between cell death around electrodes and Vo [19,56], together with the increase of tumor conductivity [18,26]. The increase of the tumor conductivity brings about

Please cite this article in press as: A. Soba, et al., Integrated analysis of the potential, electric field, temperature, pH and tissue damage generated by different electrode arrays in a tumor under electrochemical treatment, Mathematics and Computers in Simulation (2017), https://doi.org/10.1016/j.matcom.2017.11.006.

Table 1
D_{max} and RMSE values resultant from comparison by pairs of all electrode arrays for: maximum temperature (T_{max}) vs. applied voltage (Vo), maximum electric field intensity (E_{max}) vs. Vo, relative acidic tumor area vs. time and relative basic tumor area vs. time.

Comparison between electrode array modes	T_{max} vs. Vo		E_{max} vs. Vo		$A_{acidic-t}$		$A_{basic-t}$	
	D_{max} (°C)	RMSE (°C)	D_{max} (V/cm)	RMSE (V/cm)	D_{max}	RMSE	D_{max}	RMSE
A1–A2	2.82	1.381	2.61	1.663	0.07	0.051	0.03	0.024
A1–A3	1.82	0.898	2.10	1.329	0.04	0.029	0.02	0.017
A1–A4	4.50	2.235	9.20	5.955	0.03	0.023	0.02	0.018
A1–A5	4.74	2.325	3.71	2.402	0.03	0.024	0.01	0.004
A1–A6	3.64	1.968	3.70	2.405	0.03	0.023	0.01	0.004
A1–A7	0.26	0.160	2.71	1.767	0.06	0.046	0.03	0.022
A1–A8	0.33	0.198	2.71	1.753	0.06	0.045	0.03	0.022
A2–A3	1.00	0.493	0.50	0.341	0.11	0.079	0.06	0.040
A2–A4	1.68	0.856	6.61	4.292	0.04	0.028	0.01	0.006
A2–A5	1.92	0.944	6.31	4.064	0.01	0.074	0.04	0.028
A2–A6	1.07	0.625	6.31	4.067	0.01	0.074	0.04	0.028
A2–A7	3.08	1.532	5.31	3.428	0.13	0.096	0.06	0.045
A2–A8	3.15	1.574	5.31	3.415	0.13	0.096	0.06	0.045
A3–A4	2.68	1.343	7.12	4.627	0.07	0.052	0.05	0.034
A3–A5	2.92	1.432	5.80	3.731	0.01	0.006	0.02	0.012
A3–A6	1.82	1.089	5.80	3.733	0.01	0.009	0.02	0.012
A3–A7	2.08	1.049	4.82	3.095	0.03	0.017	0.01	0.007
A3–A8	2.15	1.090	4.82	3.082	0.02	0.017	0.01	0.007
A4–A5	0.24	0.104	12.90	8.357	0.06	0.047	0.03	0.022
A4–A6	0.86	0.353	12.90	8.359	0.06	0.047	0.03	0.022
A4–A7	4.76	2.387	11.91	7.721	0.09	0.069	0.06	0.039
A4–A8	4.83	2.429	11.91	7.708	0.09	0.068	0.06	0.039
A5–A6	1.10	0.449	0.03	0.012	0.00[a]	0.002	0.00[c]	0.000[e]
A5–A7	5.00	2.476	1.00	0.636	0.03	0.023	0.03	0.018
A5–A8	5.07	2.517	1.00	0.650	0.03	0.022	0.03	0.018
A6–A7	3.90	2.122	1.00	0.639	0.03	0.023	0.03	0.018
A6–A8	3.97	2.164	1.00	0.652	0.03	0.022	0.03	0.018
A7–A8	0.10	0.051	0.05	0.029	0.00[b]	0.001	0.00[d]	0.001

Ai-Aj ($i \neq j$) represents the comparison by pairs of all electrode arrays used. A1, A2, A3, A4, A5, A6, A7 and A8 depict the circular mode 1, circular mode 2, elliptic mode 1, elliptic mode 2, parabolic mode 1, parabolic mode 2, hyperbolic mode 1 and hyperbolic mode 2 arrays, respectively. T_{max} and E_{max} are the maximum temperature and electric field generated by these electrode arrays. $A_{basic-t}$ is the time dependence of relative basic area and

[a] 0.008.

[b] 0.006.

[c] 0.0007.

[d] 0.002.

[e] 0.00001.

Table 2
Relative acidic (pH < 6) and basic (pH > 8) tumor areas for 12 V and 1 h of EChT generated by the different electrode arrays and application modes tested.

Mode types	Shapes of electrode arrays			
	Circular	Elliptic	Parabolic	Hyperbolic
Mode 1	0.2301	0.2523	0.2651	0.2424
Mode 2	0.1921	0.2100	0.2657	0.2424

the increase of EChT effectiveness [25,26] and electrode polarization [35]. The chemical interaction between the electrolyte molecules and the water ions happens to breakdown the electrophoretic effect, thus activating the water ions for the DC conductivity. Besides, the increase of the electric current with voltage is explained from the increase of this physical quantity [38].

Please cite this article in press as: A. Soba, et al., Integrated analysis of the potential, electric field, temperature, pH and tissue damage generated by different electrode arrays in a tumor under electrochemical treatment, Mathematics and Computers in Simulation (2017), https://doi.org/10.1016/j.matcom.2017.11.006.

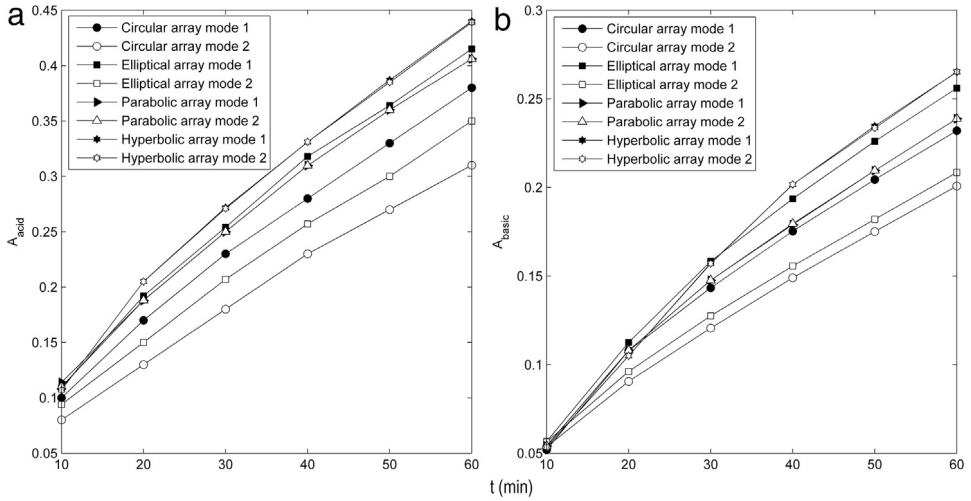

Fig. 7. (a) A_{acidic} (acidic area) versus t (time) and (b) A_{basic} (basic area) versus t induced in the tumor by electrode arrays with circular, elliptical, parabolic and hyperbolic shapes, for modes 1 and 2, and 12 V during 1 h of EChT (ECT).

In this paper, the occurrence of a stochastic resonance is not discarded; this happens for weak inputs, nonlinear systems that involve endogenous noise sources and the existence of thresholds of certain parameters [17,22]. This hypothesis may be argued because solid tumors are treated with small values of Vo (weak input: $6 \leq V\text{o} \leq 12$ V). They are nonlinear systems that involve endogenous noise sources by fluctuations and intrinsic instabilities [33]. Besides, thresholds of T (≥ 38 °C) [30,57], E (≥ 350 V/cm) [10], current density ($\geq 1\,000$ mA/m^2) [26] and pH (pH ≤ 4 around anode and pH ≥ 10 around cathode) [12,32] may be induced in the tumor, depending on EChT doses and electrode parameters.

Furthermore, noise in the tumor may be determined by multiple collisions of charged chemical species (i.e., ions, electrons, molecules) with neutral water molecules. These chemical species are accelerated by the electric field induced in the tumor, mainly around electrodes. A possible mechanism to explain these collisions is from the formation and disintegration of protonated water clusters, which takes place by adding or subtracting one water molecule [55]. This may explain, in part, the hydration and dehydration of the water around anode and cathode, respectively [32].

The above-discussed confirms the essential role of pH in the tumor necrosis, indicating that $\sigma(E, T)$, Φ and E are also influenced by pH. As a result, $\sigma(E, T)$ in Eqs. (3) and (5) should be replaced by $\sigma(E, T, \text{pH})$. This means that 2D and 3D models (realistic or not) should include $\sigma(E, T, \text{pH})$, to design adequate electrodes arrays, which are used in EChT, ECT and hyperthermia.

The underlying weakness of this numerical code is based on the use of a 2D model with lack of more realistic conditions for tissue properties. Nevertheless, 2D models are used by several reasons: (1) they are feasible for the integrated analysis of Φ, E, T and pH spatial distribution generated by these four shapes of electrode arrays. E spatial distributions in 3D models with needle electrode arrays are similar to the values obtained in 2D [1,20,41]; and both size and spatial distribution of tumor necrosis are similar around electrode for different very thin cuts of a tumor under EChT [12,25,52,51] or ECT [40] action. In addition, Φ, E, T and pH spatial distributions are difficult to measure.

Although in the literature 3D anatomically realistic models solved with COMSOL-Multiphysics and similar packages have been proposed [58], in this study, tissue realistic conditions are not considered because the electrical and biological parameters of the tumors cannot be controlled by the performing physician. Besides, preclinical [32,36,40,44] and clinical [25,27,56] studies suggest that Vo strength, electrode array geometry and electrode positioning are more important in EChT effectiveness than realistic tissue properties (electrical and anatomic). On the other hand, the spatial pattern of tissue damage in 3D potato pieces (heterogeneous and anisotropic biological tissue) adopts the same geometry of the electrode array (collinear, circular, elliptical, parabolic and hyperbolic shapes) [20]. This later is theoretically predicted in 2D and 3D homogeneous, isotropic and conductor media [15,46]. It is important

Please cite this article in press as: A. Soba, et al., Integrated analysis of the potential, electric field, temperature, pH and tissue damage generated by different electrode arrays in a tumor under electrochemical treatment, Mathematics and Computers in Simulation (2017), https://doi.org/10.1016/j.matcom.2017.11.006.

to point out that although a realistic model is not considered in this study, the mentioned in this paragraph does not mean that tissue characteristics and parameters of electrode arrays do not affect cancer cure planning.

On the other hand, as a tumor is heterogeneous and isotropic, its bulk electrical conductivity is a tensor (3×3 symmetric matrix) [35]; however, it may be diagonalized (averaged conductivity between three principal axes) [45] and therefore σ_0 may be used. The FEM code is valid when the surrounding healthy tissue (of mean basal electrical conductivity, σ_1) is also considered. Therefore, it is important to take into consideration that at Σ, Φ must satisfy the boundary conditions to ensure the continuity of the solution [26]. Moreover, the integrated analysis for 3D electrode arrays on realistic or nonrealistic tissues may be extended.

All in all, the integrated analysis of Φ, E, T and pH proves the FEM code effectiveness and it can improve understanding of electrode arrays, it can help the interpretation of experiments and it can allow the estimation of magnitudes that are difficult to measure experimentally, all of which are essential to maximize the tumor destruction with minimum damages to the organism.

In conclusion, the integrated analysis of the electric potential, electric field intensity, temperature, pH and acidic/basic areas permits to know how they depend on electrode array shape and polarization modes. This is vitally important to improve the geometrical description of electrode arrays for a better electrochemical treatment. This analysis should be included for any 2D or 3D model.

Acknowledgments

We would like to give our special thanks to the Editor in Chief and reviewers of this article for their expert help and invaluable feedback. In addition, the authors are grateful to Adrián Cabrera Ricardo, Eduardo Roca Oria, Rosa Ivette Robles Matos and Yenia Infante Frómeta for their useful discussions on the subject. This work was partially supported by the International European Cooperation in Science and Technology (COST Action TD1104) and the Cuban Ministry of Higher Education (# 6.176). Juan Bory Reyes is partially supported by the EZIME-Zacatenco, Instituto Politécnico Nacional in the framework of SIP programs. Dr. Alejandro Soba and Dr. Cecilia Suárez are researchers at CONICET.

References

[1] P. Agoramurthy, L. Campana, R. Sundararajan, Tumor electric field distribution studies using various electrodes configurations, in: Proc. ESA Annual Meeting on Electrostatics, 2011, pp. 1–8.

[2] A.R. Aguilera, L.E.B. Cabrales, L.H.M.C. Ciria, Y.S. Pérez, F.G. González, M.M. González, L.Z. Ortíz, F.S. Palencia, M.F. Salas, N.R. Bestard, G.S. González, I.B. Cabrales, Electric current density distribution in planar solid tumor and its surrounding healthy tissue generated by an electrode elliptic array used in electrotherapy, Math. Comput. Simul. 80 (2010) 1886–1902.

[3] A.R. Aguilera, L.E.B. Cabrales, H.M.C. Ciria, Y.S. Pérez, E.R. Oria, S.A. Brooks, T.R. González, Distributions of the potential and electric field of an electrode elliptic array used in electrotherapy: Analytical and numerical solutions, Math. Comput. Simul. 79 (2009) 2091–2105.

[4] V.G. Artemov, A.A. Volkov, N.N. Sysoev, Jr.A.A. Volkov, Autoionization of water: does it really occur? 2015. arXiv preprint arXiv:1508.00126.

[5] V.G. Artemov, A.A. Volkov, N.N. Sysoev, Jr. A.A. Volkov, Conductivity of aqueous HCl, NaOH and NaCl solutions: Is water just a substrate, Europhys. Lett. 109 (2015) 26002.

[6] V.G. Artemov, A.A. Volkov, N.N. Sysoev, Jr. A.A. Volkov, On autoionization and pH liquid water, Dokl. Phys. 61 (2016) 1–4.

[7] V. Bandura, S.N. Lvov, The ionization constant of water over a wide range of temperatures and densities, J. Phys. Chem. Ref. Data 35 (2006) 15–30.

[8] L.E.B. Cabrales, H.M.C. Ciria, R.N.P. Bruzón, M.S. Quevedo, R.H. Aldana, L.M. Fernández, M.F. Salas, O.G. Peña, Electrochemical treatment of mouse Ehrlich tumor with direct electric current, Bioelectromagnetics 22 (2001) 316–322.

[9] H.M.C. Ciria, M.C.S. Quevedo, L.E.B. Cabrales, R.N.P. Bruzón, M.F. Salas, O.G. Peña, T.R. González, D.S. López, J.L.M. Flores, Antitumor effectiveness of different amounts of electrical charge in Ehrlich and Fibrosarcoma Sa-37 tumors, BMC Cancer 4 (2004) 87–91.

[10] S. Čorović, L.M. Mir, D. Miklavčič, In vivo muscle electroporation threshold determination: Realistic numerical models and in vivo experiments, J. Membr. Biol. 245 (2012) 509–520.

[11] S. Čorović, M. Pavlin, D. Miklavčič, Analytical and numerical quantification and comparison of the local electric field in the tissue for different electrode configurations, Biomed. Eng. Online 6 (2007) 37.

[12] F.L. Cury, B. Bhindi, J. Rocha, E. Scarlata, K. El Jurdi, M. Ladouceur, S. Beauregard, A.K. Vijh, Y. Taguchi, S. Chevalier, Electrochemical red-ox therapy of prostate cancer in nude mice, Bioelectrochem 104 (2015) 1–9.

[13] S. Daniels, B. Rubinsky, Temperature modulation of electric fields in biological matter, PLoS One 6 (2011) e20877.

[14] R. Davalos, B. Rubinsky, Irreversible electroporation vs. cancer. US Patent Appln #2007 0043345, 2007, East Palo Alto, California (available at http://www.rexresearch.com/davalos/davalos.htm).

[15] R.M. Davidson, A. Lauritzen, S. Seneff, Biological water dynamics and entropy: A biophysical origin of cancer and other diseases, Entropy 15 (2013) 3822–3876.

[16] S.E. Fadugba, O.H. Edogbanya, S.C. Zelibe, Crank Nicolson method for solving parabolic partial differential equations, Int. J. Appl. Math. Model. 1 (2013) 8–23.
[17] L. Gammaitoni, P. Hänggi, P. Jung, F. Marchesoni, Stochastic resonance, Rev. Modern Phys. 70 (1998) 223–287.
[18] P.A. Garcia, H. Jr. Rossmeisl, R.E. Neal, T.L. Ellis, R.V. Davalos, A parametric study delineating irreversible electroporation from thermal damage based on a minimally invasive intracranial procedure, Biomed. Eng. Online 10 (2011) 34.
[19] A. Golberg, B. Rubinsky, A statistical model for multidimensional irreversible electroporation cell death in tissue, Biomed. Eng. Online 9 (2010) 13.
[20] M.M. González, C.H. Aguilar, F.A.D. Pacheco, L.E.B. Cabrales, J.B. Reyes, G.V.S. González, Electrochemical treatment: relation of the tissue damage spatial pattern with the electrodes array shape, Rev. Medisam 21 (2017) 1020.
[21] D.T. Griffin, N.F.J. Dodd, J.V. Moore, B.R. Pullan, T.V. Taylor, The effects of low level direct current therapy on a preclinical mammary carcinoma: tumor regression and systemic biochemical sequelae, Br. J. Cancer 69 (1994) 875–878.
[22] P. Hänggi, Stochastic resonance in biology. How noise can enhance detection of weak signals and help improve biological information processing, Chem. Phys. Chem. 3 (2002) 285–290.
[23] T.A. Heming, S.K. Davé, D.M. Tuazon, A.K. Chopra, J.W. Peterson, A. Bidani, Effects of extracellular pH on tumor necrosis factor-α production by resident alveolar macrophages, Clin. Sci. 101 (2001) 267–274.
[24] D.F. Jaime, G.V. Castaño, E.O. Sánchez, D.T. Pérez, J.B. Prieto, Química General 2, Ed. Félix Varela, La Habana, Cuba, 2007, pp. 448–459.
[25] M.V. Jarque, M.A.F. Mateus, F.S. Palencia, L.E.B. Cabrales, L. Jing-Hong, H.M.C. Ciria, S.C.A. Brooks, M.F. Salas, M.C.S. Quevedo, N.R. Bestard, S.G. Fernández, T.R. González, M.R. Hernández, K.C. Bordelois, First clinical experiences in Cuba over the use of electrotherapy in four patients with superficial malignant solid tumors, Rev. Medisam 11 (2007) 1.
[26] R.P. Jiménez, A.E.B. Pupo, J.M.B. Cabrales, J.A.G. Joa, L.E.B. Cabrales, J.J.G. Nava, A.R. Aguilera, M.A.O. Mateus, M.V. Jarque, S.C.A. Brooks, 3D stationary electric current density in to spherical tumor treated with low direct current, Bioelectromagnetics 32 (2011) 120–130.
[27] L. Jing-Hong, Effects of electrochemotherapy in treating patients with venous malformations, Oncotherm. J. 2 (2011) 27–39.
[28] H.B. Kim, S. Ahn, H.J. Jang, S.B. Sim, K.W. Kim, Evaluation of corrosion behaviors and surface profiles of platinum-coated electrodes by electrochemistry and complementary microscopy: biomedical implications for anticancer therapy, Micron 38 (2007) 747–753.
[29] B. Kos, A. Županič, T. Kotnik, M. Snoj, G. Serša, D. Miklavčič, Robustness of treatment planning for electrochemotherapy of deep-seated tumors, J. Membr. Biol. 236 (2010) 147–153.
[30] I. Lacković, R. Magjarević, D. Miklavčič, Three-dimensional finite-element analysis of Joule heating in electrochemotherapy and in vivo gene electrotransfer, IEEE Trans. Dielectr. Electr. Insul. 16 (2009) 1338–1347.
[31] G.H. Lee, J.D. Hwang, J.Y. Choi, H.J. Park, J.Y. Cho, An acidic pH environment increases cell death and pro-inflammatory cytokine release in osteoblasts, Int. J. Biochem. Cell Biol. 43 (2011) 1305–1317.
[32] K.H. Li, Y.L. Xin, Y.N. Gu, B.L. Xu, D.J. Fan, B.F. Ni, Effects of direct current on dog liver: possible mechanisms for tumor electrochemical treatment, Bioelectromagnetics 18 (1997) 2–7.
[33] C.F. Lo, Stochastic Gompertz model of tumour cell growth, J. Theoret. Biol. 248 (2007) 317–321.
[34] M.F. McCarty, J. Whitaker, Manipulating tumor acidification as a cancer treatment strategy, Altern. Med. Rev. 15 (2010) 264–272.
[35] D. Miklavčič, N. Pavšelj, F.X. Hart, Electric properties of tissues, in: Wiley Encyclopedia of Biomedical Engineering, John Wiley & Sons Inc, 2006, pp. 3578–3589.
[36] E. Nilsson, H. von Euler, J. Berendson, A. Thörne, P. Wersäll, I. Näslund, A.S. Lagersted, K. Narfström, J.M. Olsson, Electrochemical treatment of tumours, Bioelectromagnetics 51 (2000) 1–11.
[37] N. Olaiz, F. Maglietti, C. Suarez, F.V. Molina, D. Miklavčič, L. Mir, G. Marshall, Electrochemical treatment of tumors using a one-probe two-electrode device, Electrochim. Acta 55 (2010) 6010–6014.
[38] N. Olaiz, E. Signori, F. Maglietti, A. Soba, C. Suarez, P. Turjanski, S. Michinski, G. Marshall, Tissue damage modeling in gene electrotransfer: The role of Ph, Bioelectrochem. 100 (2014) 105–111.
[39] N. Olaiz, C. Suarez, M. Risk, F.V. Molina, G. Marshall, Tracking protein electrodenaturation fronts in the electrochemical treatment of tumors, Electrochem. Commun. 12 (2010) 94–97.
[40] A. Ongaro, L.G. Campana, M. De Mattei, F. Dughiero, M. Forzan, A. Pellati, C.R. Rossi, E. Sieni, Evaluation of the electroporation efficiency of a grid electrode for electrochemotherapy from numerical model to in vitro tests, Technol. Cancer Res. Treat. 15 (2016) 296–307.
[41] A.E.B. Pupo, M.M. González, L.E.B. Cabrales, J.J.G. Navas, E.J.R. Oria, R.P. Jiménez, J.B. Reyes, F.M. Sánchez, H.M.C. Ciria, J.M.B. Cabrales, 3d current density on tumor and surrounding healthy tissues generated by a system of straight electrode arrays, Math. Comput. Simul. 138 (2017) 49–64.
[42] A.E.B. Pupo, J.B. Reyes, L.E.B. Cabrales, J.M.B. Cabrales, Analytical and numerical solutions of the potential and electric field generated by different electrode arrays in a tumor tissue under electrotherapy, Biomed. Eng. Online 10 (2011) 85.
[43] J.I. Ramos, Picard´s iterative method for nonlinear advection reaction–diffusion equations, Appl. Math. Comput. 215 (2009) 1526–1536.
[44] R.L. Ren, N. Vora, F. Yang, J. Longmate, W. Wang, H. Sun, J.R. Li, L. Weiss, C. Staud, J.A. McDougall, C.K. Chou, Variations of dose and electrode spacing for rat breast cancer electrochemical treatment, Bioelectromagnetics 22 (2001) 205–211.
[45] M. Sekino, H. Ohsaki, S. Yamaguchi-Sekino, N. Iriguchi, S. Ueno, Low-frequency conductivity tensor of rat brain tissues inferred from diffusion MRI, Bioelectromagnetics 30 (2009) 489–499.
[46] F.H. Stilinger, Proton Transfer Reactions and Kinetics in Water, Theoretical Chemistry, in: Advances and Perspectives, vol. 3, Academic Press, New York, 1978, pp. 199–231.
[47] C. Suárez, A. Soba, F. Maglietti, N. Olaiz, G. Marshall, The role of additional pulses in electropermeabilization protocols, PLoS One 9 (2015) e113413.
[48] P. Turjanski, N. Olaiz, P. Abou-Adal, C. Suarez, M. Risk, G. Marshall, pH front tracking in the electrochemical treatment (EChT) of tumors: Experiments and simulations, Electrochim. Acta 54 (2009) 6199–6206.

Please cite this article in press as: A. Soba, et al., Integrated analysis of the potential, electric field, temperature, pH and tissue damage generated by different electrode arrays in a tumor under electrochemical treatment, Mathematics and Computers in Simulation (2017), https://doi.org/10.1016/j.matcom.2017.11.006.

[49] P. Turjanski, N. Olaiz, F. Maglietti, S. Michinski, C. Suarez, F.V. Molina, G. Marshall, The role of pH fronts in reversible electroporation, PLoS One 6 (2011) e17303.
[50] R.N. Varney, Mobility of hydrogen ions, Phys. Rev. Lett. 5 (1960) 559–560.
[51] H. von Euler, J.M. Olsson, K. Hultenby, A. Thorne, A.S. Lagerstedt, Animal models for treatment of unresectable liver tumours: a histopathologic and ultra-structural study of cellular toxic changes after electrochemical treatment in rat and dog liver, Bioelectrochemistry 59 (2003) 89–98.
[52] H. von Euler, A. Soderstedt, A. Thorne, J.M. Olsson, G. Yongqing, Cellular toxicity induced by different pH levels on the R3230AC rat mammary tumour cell line. An in vitro model for investigation of the tumour destructive properties of electrochemical treatment of tumours, Bioelectrochem. 58 (2002) 163–170.
[53] J. Werner, M. Buse, Temperature profiles with respect to inhomogeneity and geometry of the human body, J. Appl. Physiol. 65 (1988) 1110–1118.
[54] R. Wituła, E. Hetmaniok, D. Słota, A. Zielonka, Application of the Picard's iterative method for the solution of one-phase Stefan problem, Arch. Foundry Eng. 10 (2010) 83–88.
[55] T. Wróblewski, L. Ziemczonek, E. Gazda, G.P. Karwasz, Dissociation energies of protonated water clusters, Radiat. Phys. Chem. 68 (2003) 313–318.
[56] Y. Xin, H. Zhao, W. Zhang, C. Liang, Z. Wang, G. Liu, Electrochemical therapy of tumors, in: Bioelectromagnetic Medicine, Marcel Dekker Inc, 2004, pp. 709–726.
[57] S.M. Yacoob, N.S. Hassan, FDTD analysis of a noninvasive hyperthermia system for brain tumors, Biomed. Eng. Online 11 (2012) 47.
[58] A. Županič, S. Čorović, D. Miklavčič, Optimization of electrode position and electric pulse amplitude in electrochemotherapy, Radiol. Oncol. 42 (2008) 93–101.

Please cite this article in press as: A. Soba, et al., Integrated analysis of the potential, electric field, temperature, pH and tissue damage generated by different electrode arrays in a tumor under electrochemical treatment, Mathematics and Computers in Simulation (2017), https://doi.org/10.1016/j.matcom.2017.11.006.